JOURNAL OF THEORETICAL AND APPLIED MECHANICS
46, 3, pp. 565-580, Warsaw 2008

NON-LINEAR VIBRATIONS OF THE AXIALLY MOVING PAPER WEB

Krzysztof Marynowski

Technical University of Łódź, Department of Dynamics of Machines, Poland
e-mail: krzysztof.marynowski@p.lodz.pl

Non-linear vibrations of the beam-like model of an axially moving paper web with time-dependent tension have been investigated in this paper. The considered paper parameters have been determined experimentally. The beam model material is considered as the Kelvin-Voigt element. The Galerkin method and the 4-th order Runge-Kutta method have been used to solve the governing non-linear partial-differential equation. The effects of the transport speed, tension perturbation amplitude and internal damping on the dynamic behaviour of the system have been numerically investigated.

Key words: axially moving web, rheological model, non-linear dynamics

Notations

A	–	cross-section area of the web
b	–	width of the web
c	–	transport speed of the web
c_w	–	wave speed
$E = E_{MD}$	–	Young's modulus with respect to the longitudinal direction
h	–	thickness of the web
J	–	inertial moment of the cross-section
l	–	length of the web
M_x, M_y	–	sectional flexural moments with respect to the x and y axis, respectively
M_{xy}	–	sectional torsional moment
N_x, N_y	–	sectional membrane forces
N_{xy}	–	sectional shear force

q_i	–	generalized coordinate
s	–	dimensionless transport speed of the web
t	–	time
u, v, w	–	components of the displacement of a surface along the directions x, y, z, respectively
x, y, z	–	Cartesian coordinates
β	–	dimensionless coefficient of internal damping
γ	–	coefficient of internal damping
ε	–	longitudinal strain of the beam
ρ	–	density of the web material
σ	–	normal stress along the x direction
τ	–	dimensionless time.

1. Introduction

The paper is devoted to dynamics of axially moving material objects of low flexural stiffness that are referred to as webs. Problems connected with dynamical behaviour of such objects are clearly visible in paper manufacturing and printing industry. Transport speeds at which a paper web moves during manufacturing and processing can reach even 50 m/s. Under certain circumstances, such high transport speeds can lead to resonance vibrations, instability or web flattering. This behaviour can result in web folding or breaking during its motion. Changes in web tension that follow from vibrations can bring about alternations in thickness of the paper being manufactured. To ensure that the operating system is under stable working conditions, full analysis of its dynamics has to be performed. Complete knowledge of the dynamical behaviour allows the prediction and control of instabilities.

In the modelling of axially moving continua, one can use the one-dimensional string and beam theory (e.g. Wickert and Mote, 1990; Wickert, 1992; Yang and Chen, 2005) or two-dimensional plate theory (e.g. Lin, 1997; Luo and Hamidzadeh, 2004). Although the plate theory gives the most accurate description of physical phenomena that occur in the web, it is very complicated mathematically and requires time-consuming calculations. On the other hand, the results of analyses obtained so far indicate that application of the beam model of a moving web in dynamical calculations can sometimes result in satisfactory results (e.g. Moon and Wickert, 1997). One can suppose that in some dynamical calculations aiding the designing and building devices that rewind a broad web, its beam model can be useful as less complex in comparison to the plate model.

An additional argument supporting the application of the beam model is the possibility to consider various rheological models of the web material in a much simpler way than in the case of the plate model. A lot of earlier works in this field focused on dynamic investigations of string-like and beam-like axially moving elastic systems. However, paper webs need more realistic rheological models. Fung *et al.* (1998) studied transverse vibrations of an axially moving viscoelastic string subjected to a constant initial stress. Zhang and Zu (1999) investigated nonlinear vibrations of parametrically excited moving viscoelastic belts. The regular and chaotic vibrations of an axially moving viscoelastic string subjected to tensional variation were studied in Chen *et al.* (2003). Dynamic stability of an axially moving beam with time-dependent tension were investigated by using the three-parameter Zener rheological model (Marynowski and Kapitaniak, 2007).

Basing on the beam theory, equations of motion of an axially moving web with time-dependent tension have been derived in this paper. The beam model material as the Kelvin-Voigt element is considered. The Galerkin method and the 4-th order Runge-Kutta method have been used to solve the governing non-linear partial-differential equation. Non-linear vibrations of the beam-like model of an axially moving paper web with time-dependent tension have been investigated. The effects of the transport speed, tension perturbation amplitude and internal damping on the dynamic behaviour of the system have been numerically investigated.

2. Non-linear beam model of a viscoelastic web

The viscoelastic axially moving beam model of a web with a length l is considered. The beam moves at an axial velocity c. The geometry of the system and its co-ordinates are shown in Fig. 1.

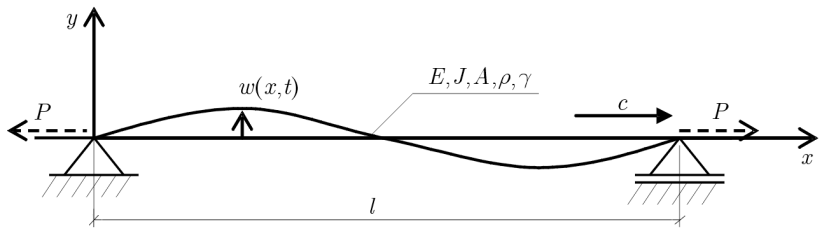

Fig. 1. Axially moving beam model of the web

Dynamics of the axially moving plate model of the web in the state of a uniform initial stress was investigated in Marynowski and Kołakowski (1999). The mathematical model that describes motion and the field of cross-sectional forces has the form of a system of three coupled differential equations of equilibrium (2.1)

$$\begin{aligned}
&\rho h(-w_{,tt} - 2cw_{,xt} - c^2 w_{,xx}) + M_{x,xx} + 2M_{xy,xy} + M_{y,yy} + q_z + \\
&\quad +(N_x w_{,x})_{,x} + (N_y w_{,y})_{,y} + (N_{xy} w_{,x})_{,y} + (N_{xy} w_{,y})_{,x} = 0 \\
&\rho h(-u_{,tt} - 2cu_{,xt} - c^2 u_{,xx}) + N_{x,x} + N_{xy,y} = 0 \\
&\rho h(-v_{,tt} - 2cv_{,xt} - c^2 v_{,xx}) + N_{xy,x} + N_{y,y} = 0
\end{aligned} \tag{2.1}$$

where q_z is the external loading.

In the case of transverse oscillations of the beam model, one should take into account only the first equation. The application of this model gives the following equation of motion in the y direction

$$\rho h_{eq}(-w_{,tt} - 2cw_{,xt} - c^2 w_{,xx}) + M_{x,xx} + (N_x w_{,x})_{,x} = 0 \tag{2.2}$$

where h_{eq} is the equivalent thickness of the beam.

The nonlinear strain component in the x direction is related to the displacement w by

$$\varepsilon(x,t) = \frac{1}{2} w_{,x}^2(x,t) \tag{2.3}$$

Dependence (2.3) shows that the geometrical type of non-linearity has been taken into consideration in the beam model of the web.

The model of internal damping introduced by Kelvin-Voigt (K-V) is shown in Fig. 2. The differential constitutive equation is as follows

$$\sigma = E\varepsilon + \gamma \varepsilon_{,t} \tag{2.4}$$

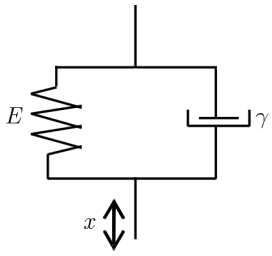

Fig. 2. Kelvin-Voigt model

Displacement of the web w is a function of the x and t variables, and substituting (2.3) into (2.4), we obtain

$$\sigma = \frac{1}{2}Ew_{,x}^2 + \gamma w_{,x}w_{,xt} + \gamma c w_{,x}w_{,xx} \tag{2.5}$$

Let us assume that the axial tension is characterised as a periodic perturbation on the steady-state tension

$$N_x = N_{x0} + N_1\cos(\Omega t) \tag{2.6}$$

where N_{x0} is the initial axial tension, N_1 – amplitude of the axial tension.

Then, Eq. (2.2) can be written in the following form

$$\begin{gathered} -w_{,tt} - 2cw_{,xt} - c^2w_{,xx} + \frac{1}{\rho h_z}M_{x,xx} + \frac{1}{\rho}\sigma_{,x}w_{,x} + \\ +[N_{x0} + N_1\cos(\Omega t)]w_{,xx} + \frac{1}{\rho}\sigma w_{,xx} = 0 \end{gathered} \tag{2.7}$$

The bending moment M is related to the displacement w by

$$M = -EJ_z w_{,xx} - J_{eq}\gamma w_{,xxt} \tag{2.8}$$

where J_{eq} is the equivalent inertial moment of the cross-section.

Using Eqs. (2.5), (2.7) and (2.8), one receives a nonlinear equation of the viscoelastic beam model with the K-V element

$$\begin{gathered} w_{,tt} + 2cw_{,xt} + c^2w_{,xx} + \frac{EJ_{eq}}{\rho A_{eq}}w_{,xxxx} + \frac{J_{eq}\gamma}{\rho A_{eq}}w_{xxxxt} - \frac{P_0 + P_1\cos(\Omega t)}{\rho A_{eq}}w_{,xx} + \\ -\frac{3}{2}\frac{E}{\rho}w_{,x}^2w_{,xx} - 2\frac{\gamma}{\rho}(w_{,x}w_{,xt}w_{,xx} + cw_{,x}w_{,xx}^2) - \frac{\gamma}{\rho}(w_{,x}^2w_{,xxt} + cw_{,x}^2w_{,xxx}) = 0 \end{gathered} \tag{2.9}$$

The boundary conditions are as follows

$$w(0,t) = w(l,t) = 0 \qquad w_{,xx}(0,t) = w_{,xx}(l,t) = 0 \tag{2.10}$$

Let the dimensionless parameters be

$$\begin{gathered} z = \frac{w}{h_{eq}} \qquad \xi = \frac{x}{l} \qquad s = \frac{c}{c_w} = c\sqrt{\frac{A_{eq}\rho}{P_0}} \\ \tau = t\frac{c_f}{l} = \frac{t}{l}\sqrt{\frac{P_0}{A_{eq}\rho}} \qquad \omega = \Omega l\sqrt{\frac{A_{eq}\rho}{P_0}} \qquad c_w = \sqrt{\frac{P_0}{A_{eq}\rho}} \end{gathered} \tag{2.11}$$

The substitution of Eq. (2.11) into Eq. (2.9) and (2.10) gives the dimensionless nonlinear equation of motion of the viscoelastic beam model

$$z_{,\tau\tau} + 2sz_{,\xi\tau} + [s^2 - 1 - \alpha\cos(\omega\tau)]z_{,\xi\xi} + \varepsilon_1 z_{,\xi\xi\xi\xi} + \beta z_{,\xi\xi\xi\xi\tau} + \\ -\frac{3}{2}\kappa z_{,\xi}^2 z_{,\xi\xi} - \eta s(2z_{,\xi\xi}^2 z_{,\xi} + z_{,\xi}^2 z_{,\xi\xi\xi}) - \eta(2z_{,\xi} z_{,\xi\tau} z_{,\xi\xi} + z_{,\xi}^2 z_{,\xi\xi\tau}) = 0 \tag{2.12}$$

where

$$\beta = \frac{J_{eq}\gamma}{l^3\sqrt{P\rho A_{eq}}} \qquad \varepsilon_1 = \frac{EJ_{eq}}{Pl^2} \qquad \kappa = \frac{Eh_{eq}^2 A_{eq}}{Pl^2} \\ \eta = \frac{\gamma h_{eq}^2 A_{eq}}{l^3\sqrt{P\rho A_{eq}}} \qquad \alpha = \frac{P_1}{P_0} \tag{2.13}$$

The boundary conditions in the dimensionless form are

$$z(0,\tau) = z(1,\tau) = 0 \qquad z_{,\xi\xi}(0,\tau) = z_{,\xi\xi}(1,\tau) = 0 \tag{2.14}$$

Equation (2.12) together with boundary conditions (2.14) constitute the mathematical model of the beam with the K-V element.

3. Solution to the problem

The problem represented by Eq.(2.12) together with boundary conditions (2.14), has been solved using the Galerkin method. The following finite series representation of the dimensionless transverse displacement has been assumed

$$z(\xi,\tau) = \sum_{i=1}^{n} \sin(i\pi\xi) q_i(\tau) \tag{3.1}$$

The 4-term finite series representation of the dimensionless transverse displacement of the beam has been taken in the numerical investigations. The even order truncations are recommended because the gyroscopic coupling in the mathematical model is taken into consideration. Substituting Eq. (3.1) into the governing equation and using the orthogonality condition, one determines a set of ordinary differential equations. To analyse the dynamic behaviour of the considered system, the set of ordinary differential equations has been integrated.

Poincaré maps and bifurcation diagrams are modern techniques used to analyse non-linear systems. These maps are convenient tools to identify the dynamical behaviour, especially chaos. In bifurcations diagrams, the dynamic behaviour may be viewed globally over a range of parameter values and compared simultaneously with various types of motion.

The Poincaré maps and bifurcation diagrams have been determined for the non-dimensional displacement of the center of the moving beam in the following form

$$v\Big(\frac{1}{2}, iT\Big) = q_1(iT) - q_3(iT) \tag{3.2}$$

where: $T = 2\pi/\omega$, $i = 1, 2, 3, \ldots$.

The fourth-order Runge-Kutta method has been used to integrate the ordinary differential equations and to analyse the dynamical behaviour of the system. The bifurcation diagrams are presented by varying the dimensionless parameters: the transport speed s, the amplitude of the tension periodic perturbation α, and the internal damping coefficient β, while the dimensionless frequency of the periodic perturbation $\omega = \pi$ is kept constant. For each set of parameters, the first 2000 points of the Poincaré map have been discarded in order to exclude transient vibration, and the displacement of the next 100 points have been plotted on the bifurcation diagrams.

4. Parameters of the paper web

The considered paper parameters have been determined in an experimental way. The experimental investigations were carried out at the Papermaking and Printing Institute in Łódź, Poland (Szewczyk *et al.*, 2006). The liner paper used in the corrugated board was employed in those investigations. The parameters describing physical properties of the liner paper are shown in Table 1.

Numerical investigations have been carried out for the beam model of the liner paper web. Parameters of the liner paper in the longitudinal direction (machine direction – MD) have been taken into account. For the data of the web: $l = 1.0\,\mathrm{m}$, $b = 1.0\,\mathrm{m}$, initial stress $N_0 = 50\,\mathrm{N/m}$, the equivalent parameters of the beam are

$$J_{eq} = \frac{D_{MD}}{E_{MD}} = 3.577 \cdot 10^{-12}\ \mathrm{m}^4 \qquad h_{eq} = \sqrt[3]{\frac{12 J_{eq}}{b}} = 3.5 \cdot 10^{-4}\ \mathrm{m} \tag{4.1}$$

Table 1. Physical parameters of paper

Parameter, notation	Liner paper
Thickness, h [mm]	0.347
Density, ρ [kg/m^3] ([g/m^2])	634.01 (220)
Young's modulus, E_{MD} [N/m^2]	$5354 \cdot 10^6$
Young's modulus, E_{CD} [N/m^2]	$2285 \cdot 10^6$
Kirchhoff's modulus, G [N/m^2]	$1186 \cdot 10^6$
Poisson's ratio, ν [–]	0.25
Poisson's ratio, ν_{yx} [–]	0.11
Plate stiffness, D_{MD} [Nm]	$19.15 \cdot 10^{-3}$
Plate stiffness, D_{CD} [Nm]	$8.18 \cdot 10^{-3}$

Then, the dimensionless parameters are

$$\varepsilon_1 = \frac{E_{MD} J_{eq}}{P_0 l^2} = 3.83 \cdot 10^{-4} \qquad \kappa = \frac{E_{MD} h_{eq}^2 A_{eq}}{P_0 l^2} = 4.595 \cdot 10^{-3} \tag{4.2}$$

5. Investigations results

The numerical investigations have been carried out for the beam model of the paper web. At first, the linearized beam model of the system was investigated. To show the dynamical behaviour of the web, natural damped oscillations of the dimensionless displacement v given by Eq. (3.2) for different values of the axial speed s of the beam model were investigated. In the subcritical region of transport speeds $(s < s_{cr})$, one can observe free flexural damped vibrations around the trivial equilibrium position (Fig. 3). In the supercritical transport speeds $(s > s_{cr})$, for small internal damping, the web experiences divergent instability and, next, flutter instability (Fig. 4). The location of instability regions of the linearized system with the K-V model of the axially moving material is shown in Fig. 5.

In dynamical analysis of the non-linear system, a parametrically unexcited system was firstly investigated. To show the dynamical behaviour of the web, a bifurcation diagram of the dimensionless displacement v given by Eq. (3.2) is presented in Fig. 6. The dimensionless transport speed s has been used as the bifurcation parameter. One can observe a supercritical pitchwork-type bifurcation at the transport speed $s = s_{b1} = 1.01$. For $s < s_{cr}$, only one attractor exists $(v = 0)$, and for $s > s_{cr}$ this critical point becomes a repeller,

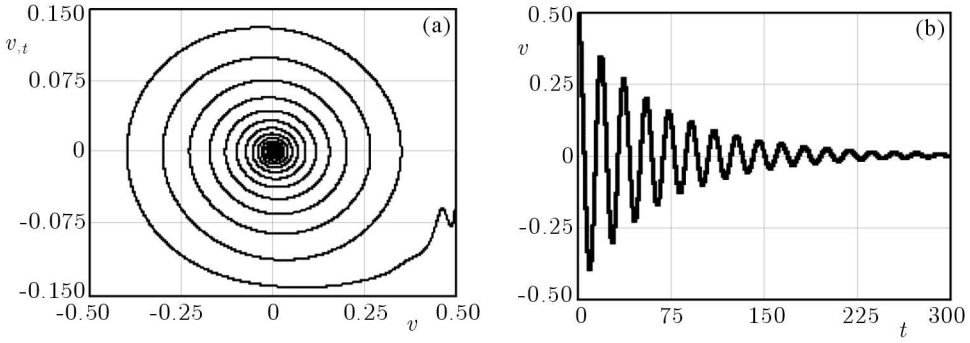

Fig. 3. Phase portrait (a) and time history (b) of the solution of the linearized system; $s = 0.95$, $\beta = 5 \cdot 10^{-4}$

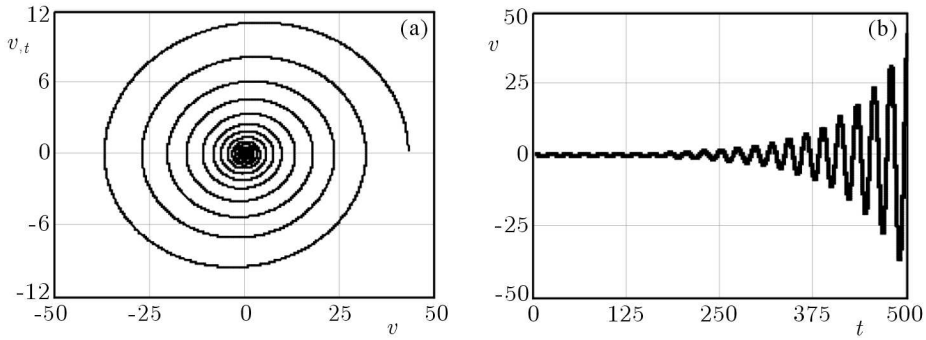

Fig. 4. Phase portrait (a) and time history (b) of the solution of the linearized system; $s = 1.04$, $\beta = 5 \cdot 10^{-4}$

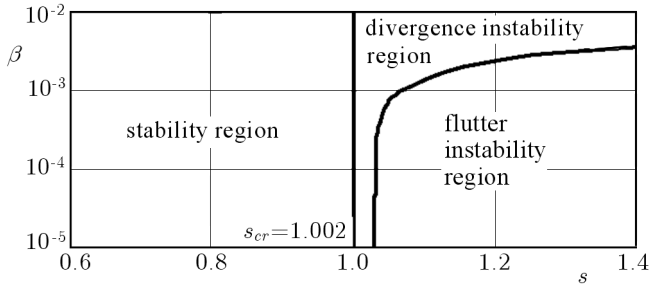

Fig. 5. Instability regions of the linearized beam model with the K-V element

and one can observe two attractors (non-zero critical points). Though the analysis of the linearized system predicts exponentially growing oscillations in the parametrically unexcited system, non-linear damped oscillations which tend to the stable critical point occur (Fig. 7).

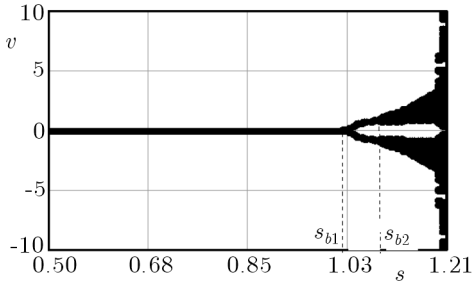

Fig. 6. Bifurcation diagram; $\beta = 5 \cdot 10^{-4}$, $\alpha = 0$

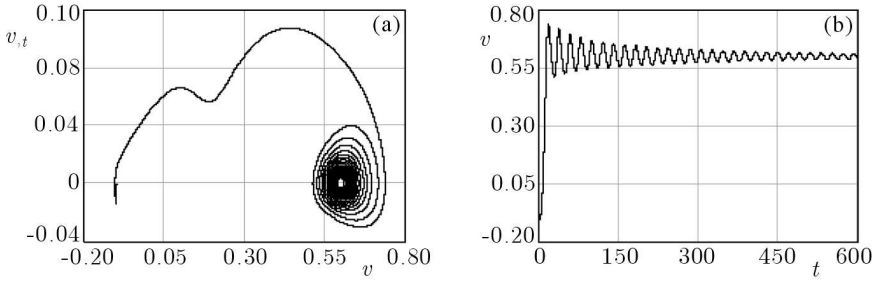

Fig. 7. Phase portrait (a) and time history (b) of the solution of the non-linear system; $s = 1.05$, $\beta = 5 \cdot 10^{-4}$

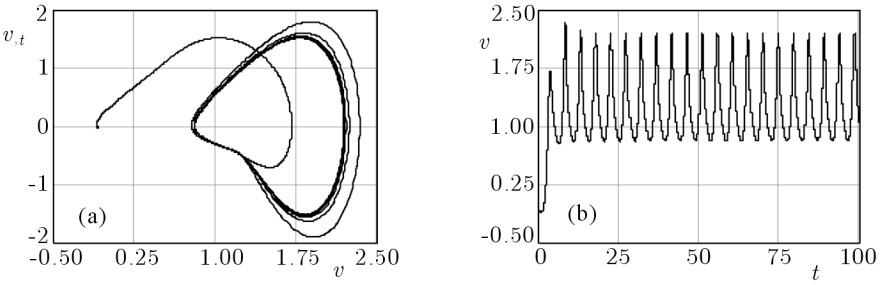

Fig. 8. Phase portrait (a) and time history (b) of the solution of the non-linear system; $s = 1.15$, $\beta = 5 \cdot 10^{-4}$

If the transport speed is further increased at $s_{b2} = 1.08$, then a Hopf-type bifurcation occurs. This bifurcation leads to the appearance a limit cycle motion (Fig. 8). It is worth to note that this region of the transport speed covers the flutter instability regions of the linearized beam model. The Poincaré map of the dimensionless displacement v in this region has a regular form, which is shown in Fig. 9.

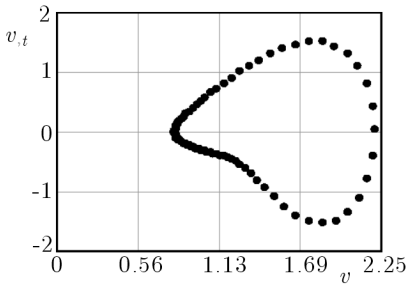

Fig. 9. Poincaré map; $s = 1.15$, $\beta = 5 \cdot 10^{-4}$, $\alpha = 0$

If the transport speed is further increased at $s_{b3} = 1.18$, then the third bifurcation occurs. At the transport speeds above the bifurcation point, the parametrically unexcited non-linear system exhibits global irregular motion.

Next, a non-linear parametrically excited system was investigated. A bifurcation diagram of the dimensionless displacement v versus the dimensionless transport speed s for specific values of the parameters α and β is shown in Fig. 10. Only the stable region of the transport speed ($s < s_{b1}$) of the parametrically unexcited system has been considered in these investigations.

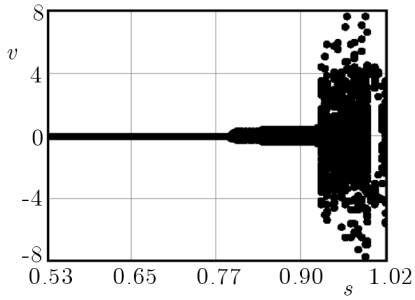

Fig. 10. Bifurcation diagram; $\beta = 5 \cdot 10^{-4}$, $\alpha = 0.5$

At the transport speed $s = 0.795$, much lower than in the unexcited case, a Hopf-type bifurcation of the zero critical point occurs. This bifurcation leads to the appearance of the limit cycle motion. Figures 11 and 12a show a phase portrait and Poincaré map of the system in this region of the transport speed. This limit cycle coexists with the zero critical point in the range $0.795 < s < 0.92$.

If the transport speed is further increased ($s > 0.92$), the limit cycle motion coexists with chaotic motion. The Poincaré map in Fig. 12b shows the dynamical behaviour of the investigated system in this region of the transport speed.

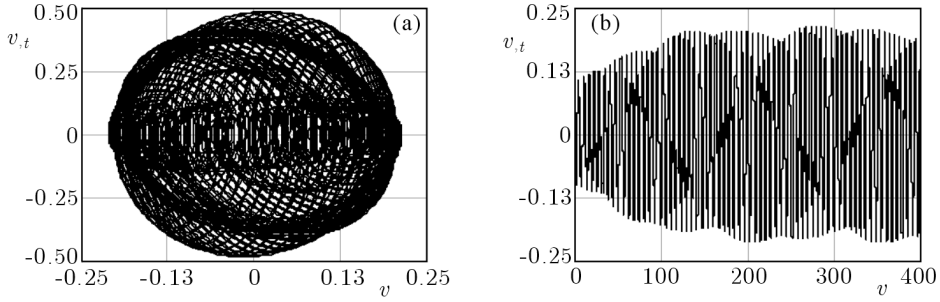

Fig. 11. Phase portrait (a) and time history of the solution of the non-linear system; $s = 0.798$, $\alpha = 0.5$, $\beta = 5 \cdot 10^{-4}$

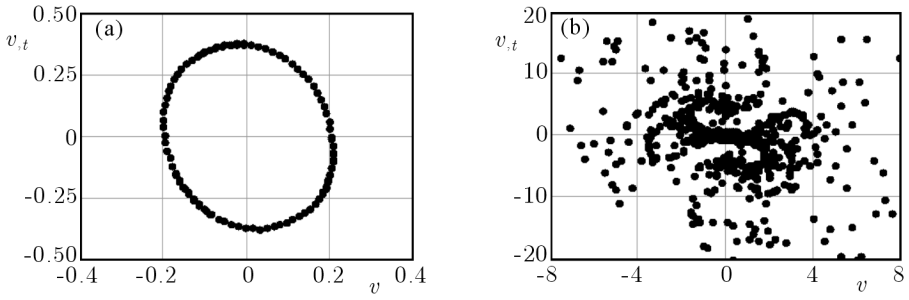

Fig. 12. Poincaré map; (a) $s = 0.798$, $\alpha = 0.5$, $\beta = 5 \cdot 10^{-4}$, (b) $s = 0.99$, $\alpha = 0.5$, $\beta = 5 \cdot 10^{-4}$

The bifurcation of the dimensionless displacement v against the non-dimensional internal damping coefficient β for fixed $s = 0.9$, $\alpha = 0.5$ is shown in Fig. 13a. When the damping coefficient has been taken as the bifurcation parameter, one can observe dynamical behaviour characteristic for non-linear systems which are determined in a multi-dimensional phase space. In this case, for small values of internal damping $(\beta < 10^{-4})$, irregular motion occurs. The Poincaré map in Fig. 13b shows the dynamical behaviour of the investigated model in this region of internal damping. With an increase in β, one can observe direct transition from a chaotic to quasi-periodic attractor (Fig. 14a).

In the region of damping $\beta > 3 \cdot 10^{-4}$, the quasi-periodic attractor coexist with the periodic attractor. Figure 14b shows the Poincaré map of a period-6 motion. Six points represent six periodic orbits in the bifurcation diagram in Fig. 13a. At $\beta = 3 \cdot 10^{-3}$, an inverse Hopf bifurcation occurs and the system is asymptotically stable with its response tending to zero.

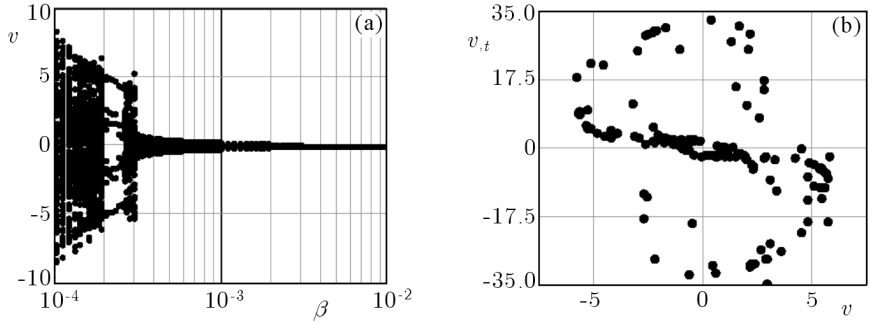

Fig. 13. (a) Bifurcation diagram, $s = 0.9$, $\alpha = 0.5$; (b) Poincaré map, $s = 0.9$, $\alpha = 0.5$, $\beta = 1.8 \cdot 10^{-4}$

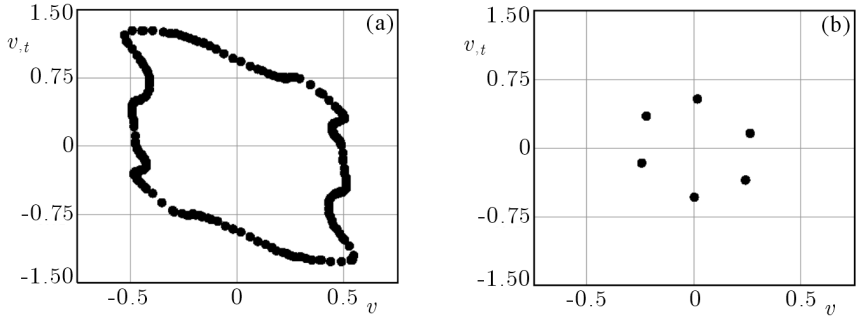

Fig. 14. Poincaré map; (a) $s = 0.9$, $\alpha = 0.5$, $\beta = 3.9 \cdot 10^{-4}$, (b) $s = 0.9$, $\alpha = 0.5$, $\beta = 7.8 \cdot 10^{-4}$

The bifurcation diagram in Fig. 15a shows Poincaré maps of the dimensionless displacement v against the perturbation amplitude α for fixed $s = 0.95$ and $\beta = 5 \cdot 10^{-4}$. In this case, the system is asymptotically stable with its response tending to zero for $\alpha < 0.2$. At the perturbation amplitude $\alpha = 0.2$, the zero critical point looses its stability and a Hopf-type bifurcation occurs. With an increase in α, quasi-periodic motion appears (Fig. 15b). At the perturbation amplitude $\alpha = 0.39$, an explosive bifurcation occurs and irregular motion appears (Fig. 15c).

6. Conclusions

The paper discusses the results of dynamical investigations of the axially moving web of liner paper obtained by means of the beam model. The two-

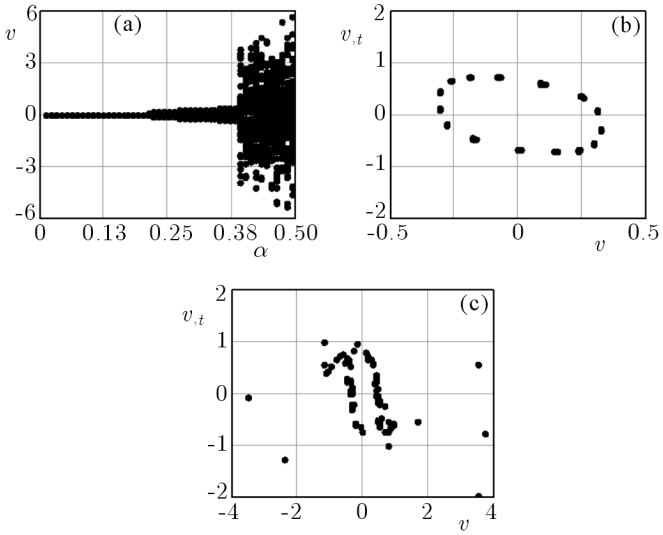

Fig. 15. Bifurcation vs. the amplitude of the periodic perturbation, $s = 0.95$, $\beta = 5 \cdot 10^{-4}$; (a) bifurcation plot, (b) Poincaré map, $\alpha = 0.38$, (c) Poincaré map, $\alpha = 0.39$

parameter Kelvin-Voigt rheological model has been employed to describe material properties of the web. The generated mathematical model in the form of a differential equation with partial derivatives has been discretized to find approximate solutions by means of the Galerkin method. The dynamical behaviour of the systems has been analysed through direct integration of the set of ordinary differential equations.

While comparing the dynamical behaviour of the nonlinear beam model with the K-V element and the nonlinear plate model analysed earlier, we can see that the transport speed at which a pitchwork-type bifurcation of the zero critical point occurs is slightly higher than that predicted by the plate model with respect to the bifurcation of the static equilibrium position. A similar dependence was also found in the investigations of the linear beam and plate models by Lin (1997).

In the case of parametric excitation of the beam model with the K-V element generated by an alternation in the tension force, the bifurcation of the zero solution occurs much earlier than the linear model predicts. First, quasi-periodic motion appears, and then with an increase in the transport speed, irregular chaotic motion takes place.

Acknowledgement

This investigation was supported by the Ministry of Science and Higher Education under grant No. 4 T07C 059 29.

References

1. CHEN L.-Q., ZHANG N.-H., ZU J.-W., 2003, The regular and chaotic vibrations of an axially moving viscoelastic string based on forth order Galerkin truncation, *Journal of Sound and Vibration*, **261**, 1, 764-773
2. FUNG R.-F., HUANG J.-S., CHEN Y.-C., YAO C.-M., 1998, Non-linear dynamic analysis of the viscoelastic string with a harmonically varying transport speed, *Computers and Structures*, **66**, 6, 777-784
3. LIN C.C., 1997, Stability and vibration characteristics of axially moving plates, *International Journal of Solid and Structures*, **34**, 24, 3179-3190
4. LUO A.C.J., HAMIDZADEH H.R., 2004, Equilibrium and buckling stability for axially traveling plates, *Comunications in Nonlinear Science and Nonlinear Simulation*, **9**, 343-360
5. MARYNOWSKI K., KOŁAKOWSKI Z., 1999, Dynamic behaviour of an axially moving thin orthotropic plate, *Journal of Theoretical and Applied Mechanics*, **37**, 1, 109-128
6. MARYNOWSKI K., KAPITANIAK T., 2007, Zener internal damping in modeling of axially moving viscoelastic beam with time-dependent tension, *International Journal of Non-Linear Mechanics*, **42**, 1, 118-131
7. MOON J., WICKERT J.A., 1997, Non-linear vibration of power transmission belts, *Journal of Sound and Vibration*, **200**, 4, 419-431
8. SZEWCZYK W., MARYNOWSKI K., TARNAWSKI W., 2006, The analysis of Young's modulus distribution in paper plane, *Fibers and Textiles in Eastern Europe*, **58**, 91-94
9. WICKERT J.A., 1992, Non-linear vibration of a traveling tensioned beam, *Int. Journal of Non-Linear Mechanics*, **27**, 3, 503-517
10. WICKERT J.A., MOTE C.D. JR, 1990, Classical vibration analysis of axially-moving continua, *Journal of Applied Mechanics ASME*, **57**, 738-744
11. YANG X.-D., CHEN L.-Q., 2005, Bifurcation and chaos of an axially accelerating viscoelastic beam, *Chaos, Solitions and Fractals*, **23**, 1, 249-258
12. ZHANG L., ZU J.W., 1999, Nonlinear vibration of parametrically excited moving belts, Part I, II, *Journal of Applied Mechanics*, **66**, 2, 396-409

Nieliniowe drgania przesuwającej się osiowo wstęgi papieru

Streszczenie

W artykule badane są nieliniowe drgania belkowego modelu przesuwającej się osiowo wstęgi papieru, będącej pod wpływem zmiennego obciążenia rozciągającego. Parametry badanego papieru zostały wyznaczone doświadczalnie. Do opisu własności reologicznych papieru został użyty model Kelvina-Voigta. Różniczkowe równania ruchu o pochodnych cząstkowych poddano procesowi dyskretyzacji, wykorzystując metodę Galerkina. Otrzymany układ równań różniczkowych zwyczajnych był całkowany metodą Runge-Kutta. Wpływ prędkości transportowej wstęgi, amplitudy obciążenia rozciągającego oraz tłumienia wewnętrznego na zachowanie dynamiczne układu był przedmiotem badań numerycznych.

Manuscript received xx yy, 2008; accepted for print April 9, 2008